JOURNAL OF GEOPHYSICAL RESEARCH, VOL. 114, D18302, doi:10.1029/2009JD011940, 2009

Ozone depletion, water vapor increase, and PSC generation at midlatitudes by the 2008 major stratospheric warming

T. Flury,[1] K. Hocke,[1,2] A. Haefele,[1] N. Kämpfer,[1,2] and R. Lehmann[3]

Received 19 February 2009; revised 7 July 2009; accepted 17 July 2009; published 23 September 2009.

[1] The ground-based microwave radiometers GROMOS and MIAWARA at Bern (Switzerland) continuously measure ozone and water vapor profiles from 20 to 70 km altitude. A major sudden stratospheric warming occurred around 19 February 2008 with minimal temperatures of 189 K at 40 hPa and maximal temperatures of 300 K at 4 hPa. During the stratospheric warming the Swiss ground-based radiometers observed a depletion of ozone and an enhancement of water vapor while NASA's CALIPSO satellite instrument measured a large PSC area over Europe. Ozone depletion in the lower stratosphere is explained by transport of ozone poor air from the cold polar vortex. The depletion of upper stratospheric ozone is caused by a sudden temperature increase of about 50 K. A simulation of a chemical box model confirms that a major fraction of the observed decrease of the ozone mixing ratio at 4 hPa can be explained by the effect of the increasing temperature on the ozone chemistry. The chemical ozone destruction is dominated by a catalytic NO_x cycle, which is more efficient at higher temperatures. The water vapor enhancement can be explained by transport processes. The rather unusual occurrence of a PSC and a sudden stratospheric warming at midlatitudes suggest that further monitoring of the Earth's middle atmosphere is required for the timely detection of unexpected problems due to ozone loss and climate change.

Citation: Flury, T., K. Hocke, A. Haefele, N. Kämpfer, and R. Lehmann (2009), Ozone depletion, water vapor increase, and PSC generation at midlatitudes by the 2008 major stratospheric warming, *J. Geophys. Res.*, *114*, D18302, doi:10.1029/2009JD011940.

1. Introduction

[2] A frequent boreal wintertime phenomenon is the sudden stratospheric warming (SSW) which is characterized by a sudden increase in temperature and a reversal of the zonal wind. *Scherhag* [1952] was the first who detected a SSW by a radiosounding over Berlin in 1952. SSWs happen in winter when the eastward mean flow of the polar stratosphere interacts with planetary waves originating in the troposphere [*Matsuno*, 1971]. Breaking and dissipation of westward propagating planetary waves at stratospheric altitudes decelerate or even reverse the prevailing eastward flow of the polar wintertime stratosphere. SSWs are often accompanied by a displacement of the polar vortex toward midlatitudes, or sometimes a splitting of the vortex is observed. A review of SSW was given by *Schoeberl* [1978].

[3] Recently major progress has been achieved in modeling and observation of SSWs. *Hoppel et al.* [2008] assimilated high-altitude temperature measurements from the satellite experiments TIMED/SABER and Aura/MLS into a global numerical weather prediction model and improved forecasting/understanding of circulation changes during the January 2006 SSW. *Coy et al.* [2009] found that the 2006 SSW was initiated by rapid growth of an upper tropospheric disturbance. Simulations by *Sun and Robinson* [2009] showed that a strong upward Eliassen-Palm (EP) flux anomaly occurs five days before a final stratospheric warming, particularly in simulations with topography. Later the zonal wind anomaly propagates from the stratosphere back to the surface. *Hirooka et al.* [2007] examined the predictability of minor and major SSWs using 1-month ensemble forecast data of the Japan Meteorological Agency. They showed that SSW are predictable at least 9 days in advance.

[4] Further simulations and observations indicated that sudden stratospheric warmings are associated with mesospheric coolings and lower thermospheric warmings [*Liu and Roble*, 2002; *Siskind et al.*, 2005; *Hoffmann et al.*, 2007]. This means that a SSW couples all atmospheric layers from the troposphere to the thermosphere. *Chau et al.* [2009] even observed variations in the equatorial ionospheric $E \times B$ drift during the SSW of 2008. Coupling processes between mean flow, planetary waves, tides, and gravity waves during a SSW are rather unexplored yet.

[5] Additionally a SSW induces changes in atmospheric composition and radiative transfer which should be taken into account. *Sonnemann et al.* [2006] simulated the effects

[1]Institute of Applied Physics, University of Bern, Bern, Switzerland.
[2]Oeschger Centre for Climate Change Research, University of Bern, Bern, Switzerland.
[3]Alfred Wegener Institute for Polar and Marine Research, Potsdam, Germany.

0148-0227/09/2009JD011940$09.00

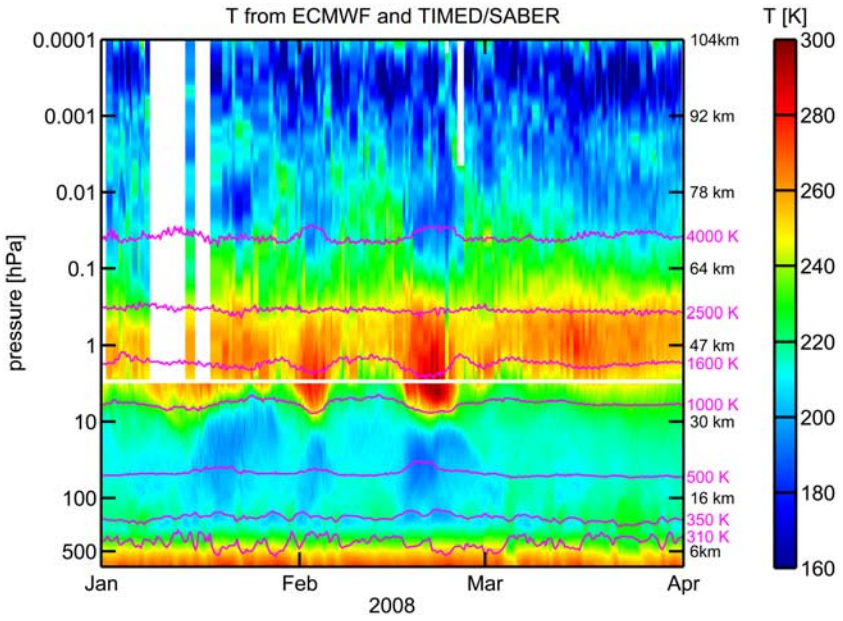

Figure 1. Time series of temperature profiles from (bottom) ECMWF and (top) TIMED/SABER over Bern (46°57′N, 7°26′E) from 1 January to 1 April 2008. Isentropes are depicted by magenta lines and show cool updraft regions and warm downdraft regions, especially during the major sudden stratospheric warming around 19 February 2008. The SSW couples atmospheric layers from the troposphere to the lower thermosphere.

of a SSW on the ozone, water vapor, and hydroxyl distribution in the mesopause region. *Liu et al.* [2009] analyzed the distribution of ozone and nitrous oxide in the middle atmosphere during SSWs and found low-ozone pockets in the simulations of the chemical transport model MOZART-3 in agreement with satellite observations. *Keil et al.* [2007] observed very low columnar total ozone over England during the SSW of 2006 and related it to ozone loss mainly in the UTLS region associated with the presence of an anticyclone at the tropopause. *Manney et al.* [2009] studied the same SSW and compared Aura/MLS trace gas measurements (H_2O, CO, CH_4 and N_2O) to a chemistry transport model from the tropopause to the lower mesosphere.

[6] The present study concentrates on the impact of the SSW of February 2008 on the ozone and water vapor distribution over Switzerland. Ozone was depleted in the whole stratosphere whereas water vapor was increased up to the mesosphere. Figure 1 shows the time series of temperature profiles over Bern (Switzerland) derived from the satellite experiment TIMED/SABER and ECMWF reanalysis for the time period 1 January 2008 to 1 April 2008. A major SSW occurred around 19 February 2008, and the SSW was clearly accompanied by updrafts and cooling of the upper troposphere, lower stratosphere, and mesosphere while downdrafts and warming took place in the midstratosphere. These observations demonstrate the vertical coupling of the whole atmosphere by a SSW, even at midlatitudes over Europe.

[7] The article is organized as follows. In section 2 we describe the instruments and data used for this study. In section 3 we report on the temperature and trace gas observations over Switzerland. Then we analyze atmospheric transport processes, wind shears, planetary waves, and the polar vortex during the February 2008 SSW. We investigate the impact of downdraft and warming on upper stratospheric ozone by using a chemical box model in section 4. In section 5 we report on a polar stratospheric cloud (PSC) over England which occurred during the SSW, and we analyze this event by means of Aura/MLS, CALIPSO, and ECMWF reanalysis data.

2. Instruments

[8] The main observations presented in this work were acquired by the ground-based microwave radiometers GROMOS (GROundbased Millimeter-wave Ozone Spectrometer) operated at Bern (46°57′N, 7°26′E, 575 m asl) and MIAWARA (MIddle Atmospheric WAter vapor RAdiometer) operated at Zimmerwald (10 km south of Bern, 46°52′N, 7°27′E, 907 m asl), Switzerland. Both are part of the Network for the Detection of Atmospheric Composition Change NDACC. GROMOS measures ozone at a frequency of 142 GHz and provides ozone profiles between 20 and 65 km with a time resolution of down to 3 minutes [*Calisesi et al.*, 2001]. MIAWARA measures the 22 GHz rotational emission line of water vapor and provides water vapor profiles from 30 to 75 km [*Deuber et al.*, 2005]. Both radiometers have a vertical resolution of about 10 km in the stratosphere. The vertical resolution is given by the FWHM of the averaging kernels. Hence features of smaller vertical extent can be observed but they are folded by the averaging kernels.

[9] Temperature data are provided by the European Center of Medium-Range Weather Forecast ECMWF, the instrument SABER (Sounding of the Atmosphere Using Broadband Emission Radiometry) on the TIMED (Thermosphere, Ionosphere, Mesosphere, Energetics and Dynamics [*Remsberg et al.*, 2003]) spacecraft and the radiosondes of

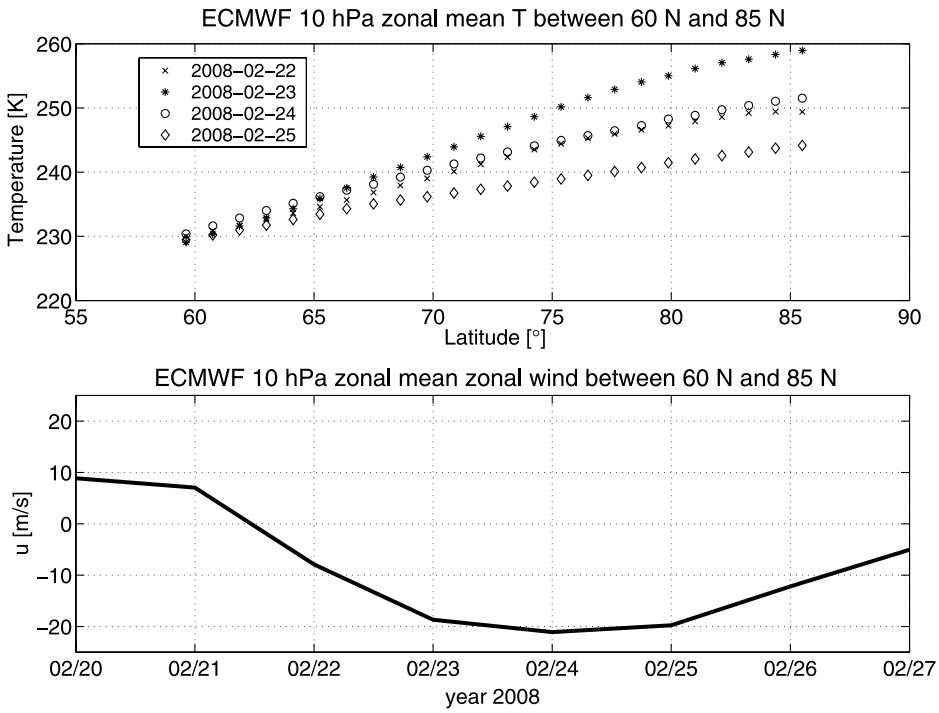

Figure 2. The major SSW of February 2008 fulfilled the WMO definition. (top) The ECMWF zonal mean temperature between 60°N and 85°N at the 10 hPa level from 22 to 25 February. The temperature increases toward the pole, which meets the first criterion for a SSW. (bottom) The ECMWF zonal mean zonal wind at 10 hPa averaged between 60°N and 85°N. On 21 February the wind becomes negative (westward) and remains negative for a week, which together with the poleward temperature increase satisfies the second criterion for a major SSW.

MeteoSwiss in Payerne (46°48′N, 6°56′E, 490 m asl), Switzerland. Moreover, data from ECMWF are utilized for the trajectory and chemistry model calculations.

[10] Data from the NASA satellite instruments Aura/MLS (Microwave Limb Sounder) and CALIPSO are used to confirm our O_3 and H_2O data and the presence of a PSC and O_3 depleting substances. Aura/MLS is a passive microwave instrument that measures different trace gases and temperature [*Waters et al.*, 2006] in the middle atmosphere. Due to its limb sounding technique Aura/MLS has a better vertical resolution than GROMOS and MIAWARA which is between 3 and 6 km for stratospheric O_3 and better than 4 km for H_2O [*Froidevaux et al.*, 2008; *Lambert et al.*, 2007]. The H_2O profiles of Aura/MLS have been validated with our instrument MIAWARA [*Haefele et al.*, 2009]. CALIOP (Cloud-Aerosol LIdar with Orthogonal Polarization) is the instrument on the CALIPSO (Cloud-Aerosol Lidar and Infrared Pathfinder Satellite Observations) satellite and is a LIDAR which measures the backscatter of clouds and aerosols [*Winker et al.*, 2007]. CALIPSO has been validated by *McGill et al.* [2007].

3. Observations

3.1. Is the February 2008 Event a Major Stratospheric Warming?

[11] In order to standardize the use of the terms "major" and "minor" stratospheric warmings the World Meteorological Organization's (WMO) Commision for Atmospheric Sciences has adopted the following definitions as can be read in the work of *McInturff* [1978].

[12] "1. A stratospheric warming is called minor if a significant temperature increase is observed (i.e., at least 25 degrees in a period of a week or less) at any stratospheric level in any area of the wintertime hemisphere, measured by radiosonde or rocketsonde data and/or indicated by satellite data; and if criteria for major warmings are not met.

[13] 2. A stratospheric warming can be said to be major if at 10 hPa or below the latitudinal mean temperature increases poleward from 60 degrees latitude and an associated circulation reversal is observed (i.e. mean eastward winds poleward of 60° latitude are succeeded by mean westward winds in the same area)."

[14] We intentionally use the WMO definition of *McInturff* [1978] because there seem to exist several WMO definitions of a major stratospheric warming while the original WMO document seems to be unknown. Many authors refer to a WMO definition without giving any literature reference. Hence the definitions differ slightly. There is agreement about the temperature increase poleward of 60°N but some quote that it has to last for at least 4 consecutive days [*Chaffey and Fyfe*, 2001] others say that it must last for 5 days [*Limpasuvan et al.*, 2004]. No time duration is defined by *McInturff* [1978], *Labitzke* [1981] and *Schoeberl* [1978]. The second criterion about the wind reversal is also controverse: The latter three authors use a circulation reversal poleward of 60 degrees whereas *Charlton and Polvani* [2007] defined that the mean zonal winds must become westward at 60°N and *Limpasuvan*

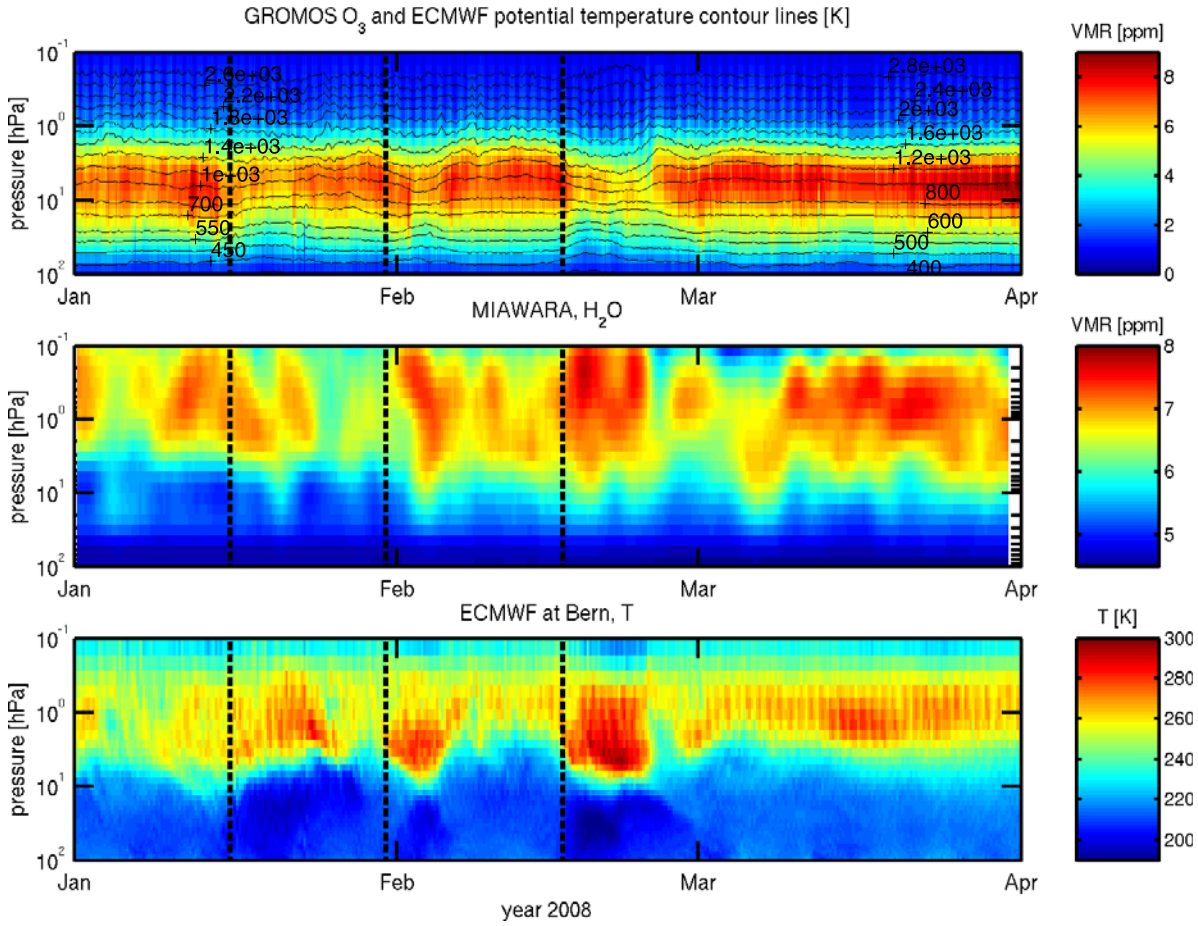

Figure 3. O_3, H_2O, and temperature profiles at Bern from January to April 2008 as a function of pressure. (top) O_3 VMR as measured by GROMOS with contours of isentropes. (middle) H_2O VMR as measured by MIAWARA. (bottom) ECMWF temperatures. Three SSWs occurred (start marked by dashed vertical lines). The first started on 16 January, the second on 31 January, and the last on 17 February, which was a major warming. All three warming events were accompanied by a lower stratospheric cooling due to a displacement of the polar vortex toward Bern. O_3 reduction and H_2O enhancement occurs during the major SSW.

et al. [2004] used the same but at 65°N (for the Northern Hemisphere).

[15] Now we test if the SSW event around 19 February 2008 observed at Bern can be categorized as a major warming according to the definition given higher up. Zonal-mean temperatures are derived between 60°N and 85°N from the global temperature field at 10 hPa from ECMWF reanalyis and temporally averaged over the time interval 22–25 February. Further the daily ECMWF zonal mean zonal wind between 60°N and 85°N at 10 hPa is calculated with area weighting by the cosine of the latitude. Figure 2 shows these temperature and zonal wind data. The upper panel displays the daily averaged ECMWF zonal mean temperature between 60°N and 85°N, spaced by 1.125°, at the 10 hPa level from 22 February to 25 February. The temperature increases indeed poleward which meets the first criterion for a major stratospheric warming. The lower panel shows the daily average of the zonal mean zonal wind at 10 hPa between 60°N and 85°N. On 21 February the wind becomes negative (westward) and remains negative for a week. Hence the second criterion for a major SSW is also fulfilled as it meets the WMO definition of *McInturff* [1978] for the reversal of the zonal mean zonal wind.

3.2. Stratospheric Warming and Cooling

[16] During the northern hemispheric winter 2007/2008 two minor stratospheric warmings occurred in January and beginning of February and one major sudden stratospheric warming toward the end of February. Figure 3 shows a time series of O_3 and H_2O measured by our instruments and ECMWF temperatures from 100 hPa to 0.1 hPa over Bern, Switzerland. The onset of the three events is highlighted by vertical dashed lines. Simultaneously to the upper stratospheric warmings the temperature decreased in the lower stratosphere below 10 hPa. The contour lines superposed on the O_3 plot show the evolution of potential temperature Θ. A distinctive upwelling of isentropes is observed for Θ between 400 K and 550 K and a downwelling between Θ = 1000 K and 2000 K during the major SSW.

[17] In the lower stratosphere at 40 hPa temperatures fell to a minimum of 189 K on 21 February. In the upper

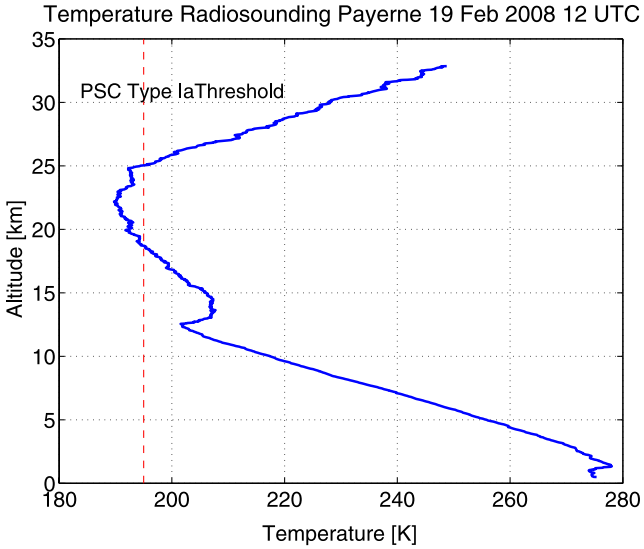

Figure 4. Temperature profile from a MeteoSwiss radiosonde at Payerne (46°48′N, 6°56′E, 40 km next to Bern) on 19 February 2008. The temperature between 19 and 25 km is below 195 K (threshold for the formation of PSC type 1a clouds).

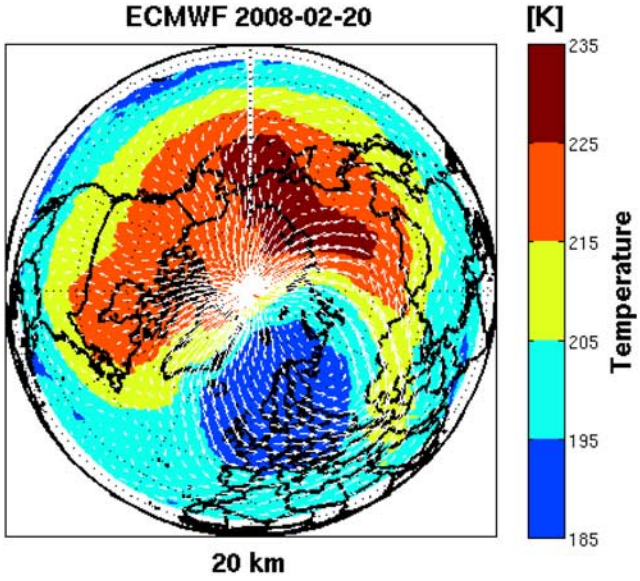

Figure 5. ECMWF temperatures at 55 hPa (∼20 km) on 20 February 12 UTC. A wave 1 structure is evident with the cold air lying above Europe. White vectors denote the horizontal wind direction in arbitrary units.

stratosphere at 4 hPa the maximum temperature of 300 K was recorded 1 day later on 22 February. The consequence of the warming was that the stratopause altitude dropped from 52 km to 38 km in 2 days between 17 February and 19 February, this drop can be estimated in Figure 1.

[18] A detailed temperature profile recorded by a MeteoSwiss radiosonde from Payerne (46°48′N, 6°56′E) is shown in Figure 4. Payerne is situated 40 km southwest of Bern. The weather balloon reached an altitude of 33 km and encountered temperatures below 195 K in the layer from 19 to 25 km. 195 K is the threshold temperature for the formation of Nitric Acid Trihydrate (NAT) PSCs of type 1a. The exact threshold temperature is a function of the water vapor (H_2O) and nitric acid (HNO_3) volume mixing ratio (VMR [*Hanson and Mauersberger*, 1988]). The minimum temperature was 190 K at 23 km altitude. Since 1995 stratospheric temperatures as low as in this case were observed over Payerne only on four occasions, namely in January 1995, January 2004, January 2006 and February 2008. Those cold events were all recorded during a SSW period as identified by *Charlton and Polvani* [2007] and *Charyulu et al.* [2007].

[19] Figure 5 shows the hemispheric distribution of stratospheric temperatures and horizontal wind direction at 55 hPa (∼20 km) and Figure 6 the same quantities but at 4 hPa (∼37 km). There is a wave 1 structure with a cold pole over Europe and warm temperatures over the Aleuts at 55 hPa and an almost opposite structure at 4 hPa. This is a sign of the vertical distortion of the polar vortex and implies an exchange of air masses between subtropical and polar latitudes. The stratospheric warming over Europe at 4 hPa is the consequece of air mass transport from lower latitudes as already reported by *Kleinböhl et al.* [2005]. Air is advected from the south toward Europe, as it sinks, it further heats up adiabatically. The downward motion is also visible in the potential temperature contour lines in Figure 3, which sank during the SSW.

[20] Figure 7 illustrates a two-dimensional shape of the polar vortex visualized for the major SSW event on different altitude levels. The modified potential vorticity [*Lait*, 1994] is plotted on layers spaced by 4 km starting at 18 km and ending at 50 km altitude, red color marks the location of the polar vortex and the blue vertical line shows the coordinates of Bern. The polar vortex is shifted to Bern between 18 and 34 km, where the cooling was observed. Above 34 km the

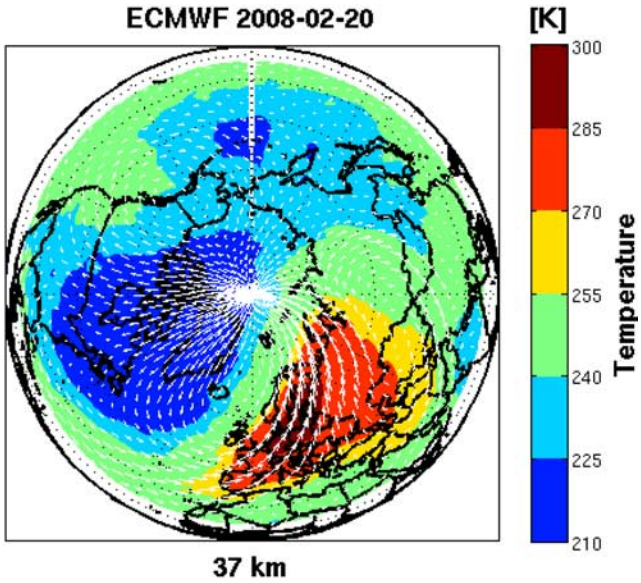

Figure 6. ECMWF temperatures at 4 hPa (∼37 km). The wave 1 structure is still visible, but the cold and hot poles are shifted by 180°. Warm air is over Europe. White vectors denote horizontal winds as before.

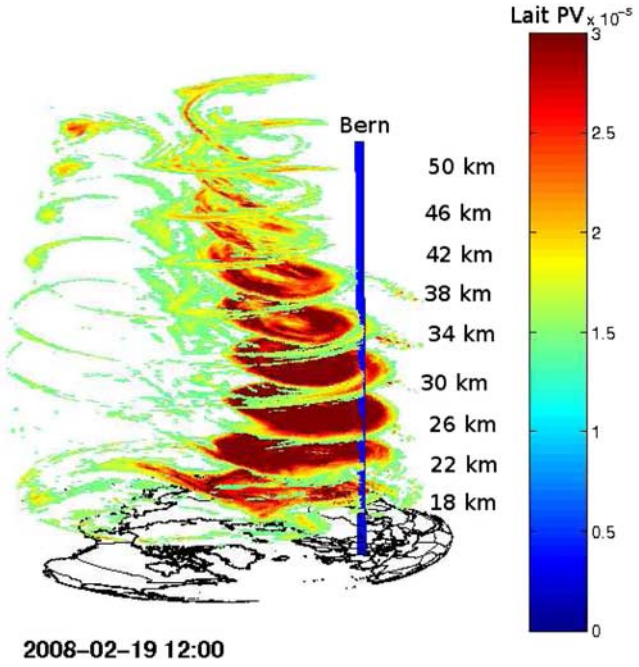

Figure 7. Polar vortex shift to midlatitudes during the major SSW of 19 February 2008. Modified potential vorticity (Lait PV) plotted every 4 km altitude starting at 18 km. The blue vertical line indicates the location of Bern. Red areas mark the location of the polar vortex. The column above Bern lies within the vortex up to 36 km and is outside above.

vortex is no longer over Bern and it dissipates with increasing height.

3.3. Ozone Depletion and Water Vapor Enhancement

[21] The ground-based microwave radiometer GROMOS continuously measured ozone over Bern from January to April 2008. Volume mixing ratio profiles are shown in the upper panel of Figure 3. Simultaneously the ground based microwave radiometer MIAWARA observed water vapor in the middle atmosphere over Bern. The H_2O VMR is illustrated in the middle panel of Figure 3. The synthesis of all three panels of Figure 3 is discussed in the following parts.

[22] A strong link between O_3 and temperature (T) is present in the lower stratosphere at 55 hPa where the temporal variations of O_3 and T are correlated. The correlation at 55 hPa is displayed in detail in Figure 8. On the upper panel GROMOS data are plotted with a solid line together with Aura/MLS version 2.2 ozone (X). The satellite measurements were chosen to be not further away from Bern as 2° in latitude and longitude. During all 3 SSWs, O_3 VMR decreases in phase with the temperature. As soon as T increases, O_3 increases as well. During the major SSW the temperature dropped from 210 K to 192 K and coincidently O_3 VMR decreased by 23% from 2.6 ppm to 2 ppm. On 20 February temperature begins to increase again and so does ozone until a maximum O_3 VMR of 3.3 ppm is reached at the same time as a temperature maximum of 218 K in the beginning of March. The correlation of MLS and GROMOS is very good although GROMOS slightly underestimates the ozone values of MLS.

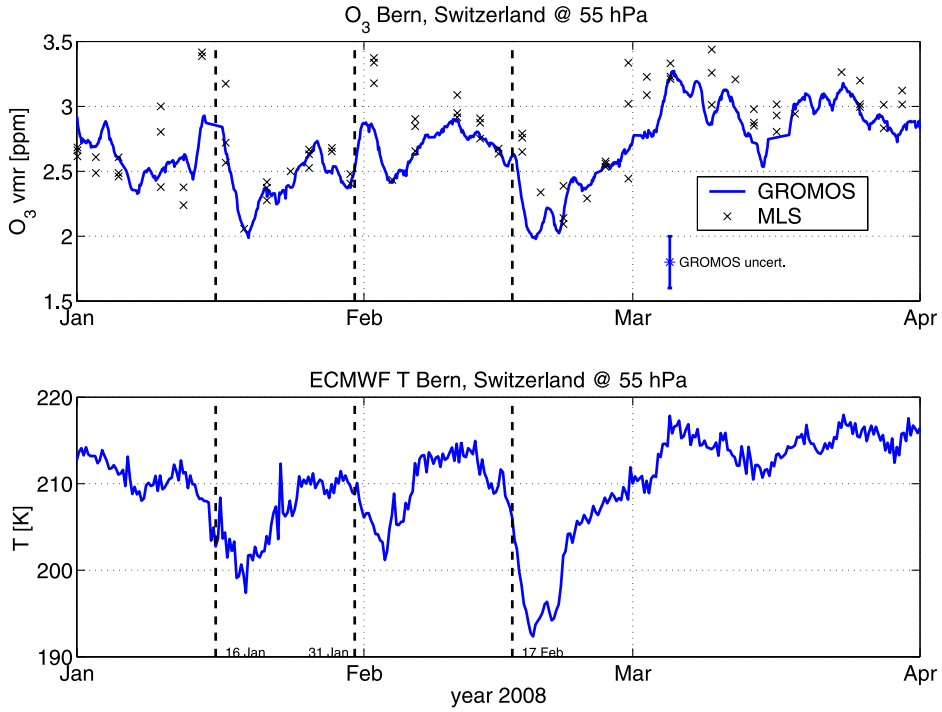

Figure 8. (top) O_3 VMR measured by GROMOS and Aura/MLS. (bottom) ECMWF temperatures at 55 hPa (~20 km). Ozone and temperature are correlated: O_3 VMR decreases with decreasing temperatures. During the major SSW on 19 February the temperature was below PSC type 1a threshold of 195 K. Dashed lines are starting dates of the SSWs.

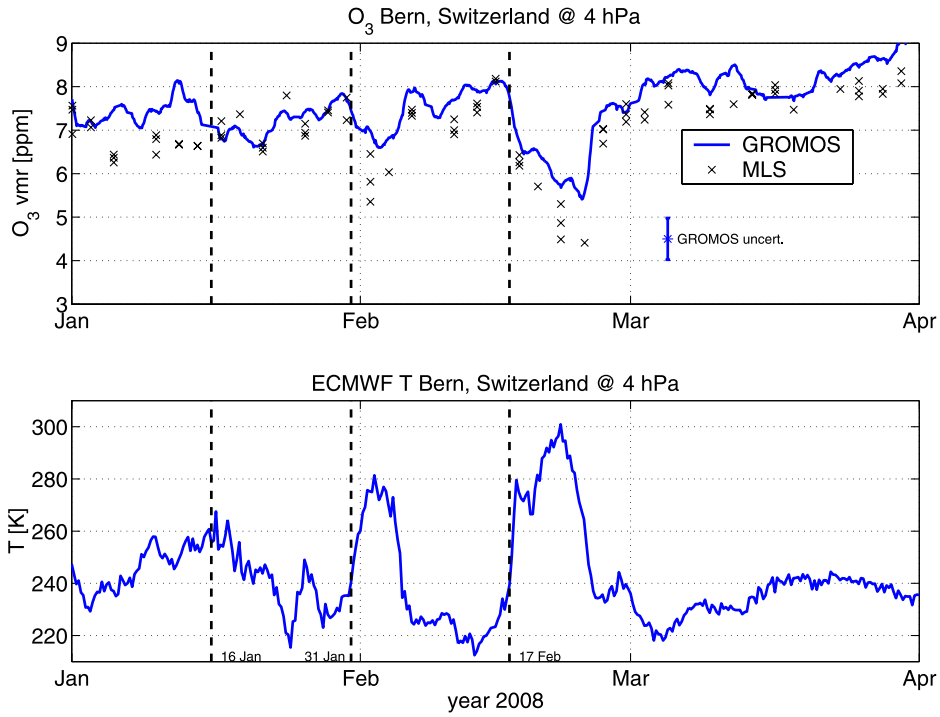

Figure 9. The same quantities as before but at 4 hPa (∼37 km). Ozone and temperature are anticorrelated: O_3 VMR decreases with increasing temperatures. Minimum O_3 VMR is reached shortly after the warmest temperature around 22 February.

[23] Figure 9 illustrates the same quantities but at 4 hPa in the upper stratosphere. O_3 shows anticorrelation with T what is opposite to the behavior at 55 hPa. As soon as T exceeds 250 K the O_3 VMR drops rapidly with still increasing temperature. This happened during SSW of 31 January and during the major SSW. During the major SSW the temperature increased from 215 K to 300 K and the O_3 VMR decreased from 8 ppm to 5.5 ppm which is a reduction of 31%. The ozone recovery starts with the decline of T and reaches prewarming VMR of 7.5 ppm in the beginning of March. The correlation of MLS and GROMOS is again good. Except during the SSW the difference is larger, this could be due to increased atmospheric variablility on small scales associated with the edge of the polar vortex. The polar vortex was tilted with altitude and the MLS sounding volume differs from the slant column volume seen by GROMOS over Bern. In summary overall ozone is depleted by more than 30% in the lower and upper stratosphere during the SSW events.

[24] MIAWARA shows an enhancement of H_2O as a reaction to the SSW as is visible in Figure 3. Figure 10 shows the relative variations of H_2O VMR in three layers (25–10 hPa, 10–1 hPa and 1–0.1 hPa) with respect to a January to April average. The solid lines represent MIAWARA measurements while the dashed lines are from Aura/MLS version 2.2. MLS H_2O profiles were chosen to meet the same coincidence criterion as for O_3 explained above. The uncertainty of MIAWARA is 10%. An anomaly, rather than an absolute representation, was chosen because MIAWARA has low sensitivity in the level 25–10 hPa and a bias of up to 10% to Aura/MLS [*Haefele et al.*, 2009]. In all 3 cases a local maximum is reached by MIAWARA a few days after the onset of the SSW at each level except for the first SSW in the mesosphere (1 to 0.1 hPa). The most prominent increase happened in the lower mesosphere, to see in the uppermost panel, where a relative increase of 16% is observed starting before the second SSW and also an increase of 15% for the major SSW. The satellite limb sounding instrument is much more sensitive to the lower stratosphere than MIAWARA, hence it observed a more pronounced increase. The correlation of MLS and MIAWARA is good in the lower and upper panel. The two lower height ranges are not completely independent in the MIAWARA retrieval, hence both curves look similar. The 19 February is a remarkable day since at each level a maximum was reached after which the H_2O VMR decreased again. At the same day minimum temperatures were recorded by the MeteoSwiss radiosonde shown in Figure 4.

3.4. Air Parcel Trajectories and Strong Wind Shear

[25] Major SSWs are characterized by either a split or a shift of the polar vortex toward lower latitudes. According to the 50 year statistical analysis of *Charlton and Polvani* [2007] a shift is more often observed. In the present case the polar vortex was shifted toward central Europe (Figure 7).

[26] Figure 11 shows 3 days backward trajectories ending on 20 February 2008 at 12 UTC over Bern. Trajectories are calculated by the TomTom model [*Flury*, 2008] for the isentropes 500 K and 1400 K. The model is set up in a Matlab code and interpolates directly ECMWF wind data on the air parcel location. Isentropic motion is assumed and we use a one hour time step. Matlab accesses directly the ECMWF data stored in our institute's MySQL database

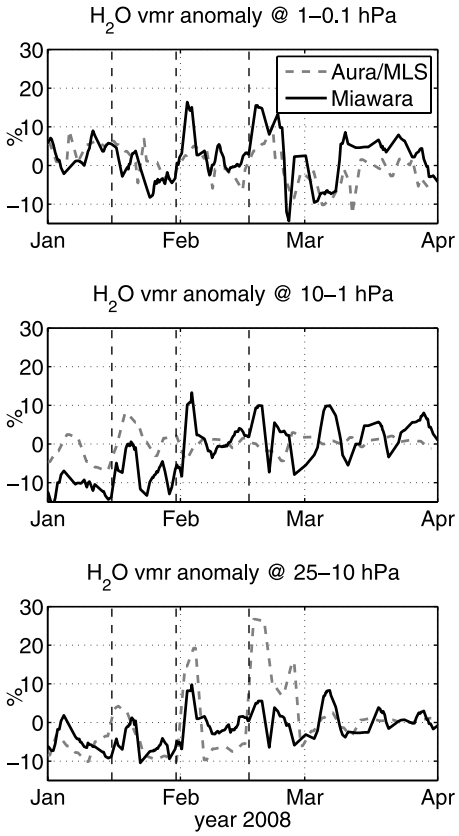

Figure 10. Relative variations of H_2O VMR observed by MIAWARA (solid curve) and Aura/MLS (dashed curve) in three different layers (lower and upper stratosphere and lower mesosphere). MIAWARA is smoothed with a 2-day running mean. Vertical dashed lines correspond to the SSW starting dates. A local maximum is reached by MIAWARA a few days after each onset of a SSW.

and calculates trajectories with the equation of motion. An efficient handling of large data fields is important for trajectory models. Our experience indicates that MySQL is ideal for the extensive administrative and search tasks connected with trajectory calculations. Comparison to the HYSPLIT (NOAA) model [*Draxler and Hess*, 1998] and Goddard Automailer [*Schoeberl and Sparling*, 1994] showed an agreement of better than 200 km for 3 day trajectories in the lower stratosphere.

[27] In the lower stratosphere at Θ = 500 K, displayed by the black trajectory in Figure 11, cold air was brought to Switzerland. The air parcel started on 17 February over Siberia and showed strong upwelling over the north Atlantic Ocean between Greenland and Switzerland. This adiabatic rise led to prominent cooling down to 189 K over France. The polar origin of the air in the lower stratosphere over Bern illustrates the displacement of the polar vortex toward midlatitudes.

[28] The opposite behavior is found for the air parcel simulated on Θ = 1400 K represented by colored asterisks. The color represents the temperature of the air parcel. The air was advected from subtropical latitudes over the US and underwent strong downwelling on the last 12 hours before Bern. The air parcel sank from 41 to 36.7 km at the arrival over Bern. This led to adiabatic heating by 40 K and explains the warming over Bern. In between these very different trajectories is a layer of strong wind shear.

[29] The two wind regimes are illustrated in Figure 12, which shows the horizontal wind profile on the 8°E meridian of Bern as a function of latitude from the tropics to the pole. The contour lines represent meridional wind speed, where positive values mean northward. The color displays the zonal component with positive values being eastward. Two maxima of the so-called polar night jet are visible: One is at 30 km and 40°N and the second spreads from 50 to 65 km between 55° and 60°N. The polar night jet marks the edge of the polar vortex which is normally located north of 60°N in winter. Hence one can see the displacement of the vortex toward the latitude of Bern which is marked by the vertical black line. Further one observes the reversal of the zonal wind to westward between 20 and 60 km altitude north of 75°N, which is characteristic for a major SSW.

[30] The observed H_2O enhancement during the SSW shown in Figure 10 can partly be explained by transport. The distribution of water vapor depends on season, latitude and altitude (e.g., Aura/MLS global maps available at the Webpage http://mls.jpl.nasa.gov/data/gallery.php). *Flury et al.* [2008] showed that water vapor variations in the lower mesosphere can be traced back by means of trajectory calculations. The significant enhancement recorded in the lower mesosphere between 1 and 0.1 hPa (48–64 km) can thus be evaluated using TomTom. Mesospheric air was of subtropical origin where the H_2O VMR was greater than over Bern. MIAWARA thus observed a transport of water vapor rich air to Bern. In the lower stratosphere polar vortex air was brought to Bern. H_2O VMR is higher inside the polar vortex than outside due to downward vertical advection. Hence air of higher H_2O VMR was transported to Bern.

4. Modeling of the Temperature Sensitivity of Ozone

[31] The ozone depletion at 4 hPa during the major SSW starts on 17 February as displayed in Figure 9. Already 2 days earlier O_3 started to decrease higher up at 1.8 hPa, suggesting that the disturbance propagates downward in the atmosphere. The recovery starts as soon as the temperature decreases again. At this altitude an anticorrelation of O_3 VMR and temperature is evident.

[32] A major fraction of the O_3 change can be explained by the effect of the changing temperature on the ozone chemistry. In order to demonstrate this, we ran a chemical box model with the parameters temperature and pressure as encountered on the Θ = 1400 K trajectory shown in Figure 11. Chemical initialization was made with ozone VMR from ECMWF. For NO_x we used the nighttime zonal average between 30°N and 40°N of NO_2 for February 2008 measured by MIPAS [*Wetzel et al.*, 2007]. MIPAS (Michelson Interferometer for Passive Atmospheric Sounding) is a spaceborne infrared limb sounder on the ESA's ENVISAT satellite. Nighttime NO_2 can be used as a good approximation for NO_x as NO is rapidly transformed to NO_2 during night. All other initial mixing ratios such as chlorine containing species were taken from the work of *Brasseur et al.* [1999], section C. The model contains 175 reactions

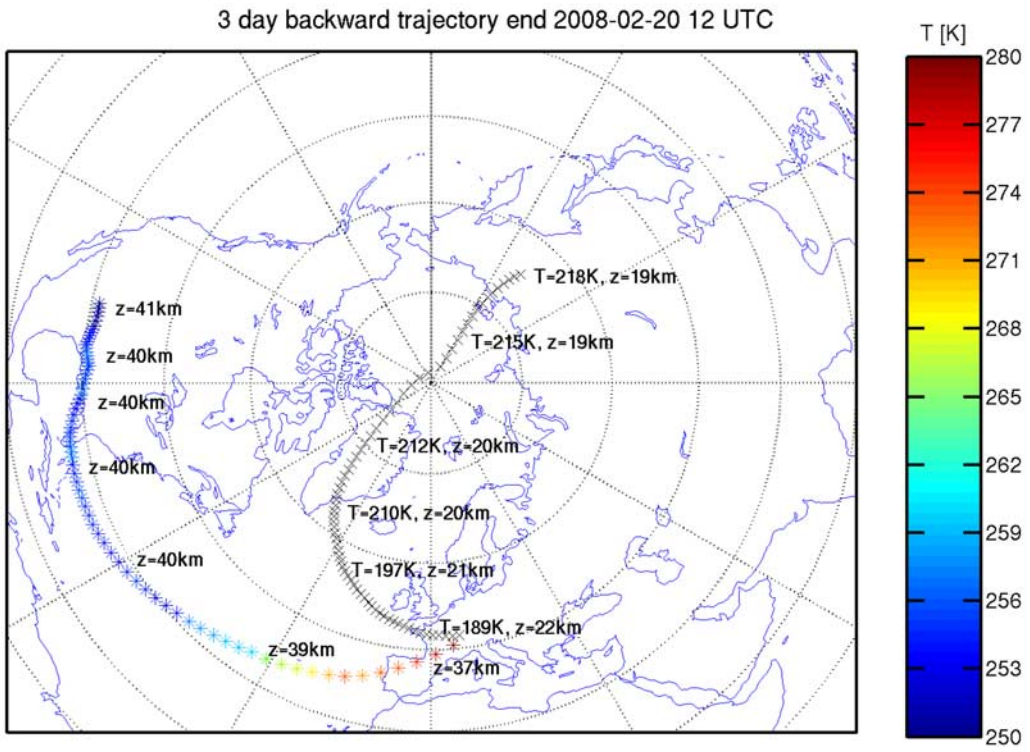

Figure 11. Three-day backward trajectories arriving at Bern on 20 February 2008 at 12 UTC. The black trajectory is calculated on the 500 K isentrope by the TomTom model. Every 12 hours the ECMWF temperature and height of the air parcel are labeled. Please notice the upwelling and cooling between Greenland and Ireland. Temperatures were below the PSC threshold of 195 K between the UK and Switzerland. The colored trajectory is calculated for the Θ = 1400 K isentrope. Colors of the symbols denote the air parcel's temperature. Strong downwelling (parcel sinks from 40 to 37 km) and adiabatic heating (→SSW) of the air parcel occur before arrival at Bern. The trajectories show the coincidence of lower stratospheric cooling and upper stratospheric warming over Bern.

among 48 chemical species, with rate constants according to *Sander et al.* [2006].

[33] The runs were carried out along the 1400 K isentropic trajectory, which brought air from southern Texas to Switzerland within 3 days. In order to differentiate between the effect of increasing temperature and descent along the trajectory on the O_3 budget, several runs were made with different assumptions regarding temperature and altitude of the ozone containing air parcel.

[34] Figure 13 displays O_3 VMR calculated along the trajectory. Yellow areas mark daytime (solar zenith angle <90°), i.e. time during which sun photolysis is active. The two red curves are initialized with ECMWF O_3, plotted by green dots, calculated for the location of the air parcel's starting point at 2.35 hPa. The red solid line (Descent, warming) represents the simulation along the original trajectory, i.e. with its changing temperature and pressure. It shows how the warming during the last few hours decreases the VMR by about 0.5 ppm. The red dashed line (Descent, no warming) simulates an air parcel on the original trajectory, but the temperature is kept at the initial cold value of 248 K. This simulation shows that descent without warming even increases the O_3 VMR.

[35] The blue curves on Figure 13 represent a simulation of the O_3 VMR along a trajectory on the constant pressure level of 4 hPa, corresponding to the arrival height of the original trajectory above Bern. The latitudes and longitudes for this simulation were taken from the original trajectory. The run was initialized with the ECMWF O_3 VMR at 4 hPa on the parcel's starting point. The temperature dependence is again obvious. The dash-dotted blue line (No descent, warming) decreases rapidly by 0.6 ppm during the strong warming at the end. On the other hand, the O_3 VMR represented by the dashed line (No descent, no warming, i.e. constant temperature of 248 K) remains nearly constant. The latter run represents a "usual" trajectory arriving above Bern (without SSW). A comparison of this run with the "Descent, warming" run along the original descending trajecory illustrates the total effect of the SSW on ozone. In order to separate the effect of the temperature increase on ozone, we have to compare the curves "Descent, warming" with "Descent, no warming" or "No descent, warming" with "No descent, no warming." Given these simulations we can argue that, under the conditions considered, approximately 2/3 of the encountered O_3 decrease during the SSW can be attributed to the temperature increase.

[36] The strong temperature sensitivity of ozone may be explained as follows: The ozone mixing ratio is determined by the ozone production (O_2 photolysis, insensitive to temperature) and ozone destruction. The main catalytic ozone destruction cycles are NO_x and ClO_x cycles. Minor contributions to ozone loss are added by the Chapman cycle

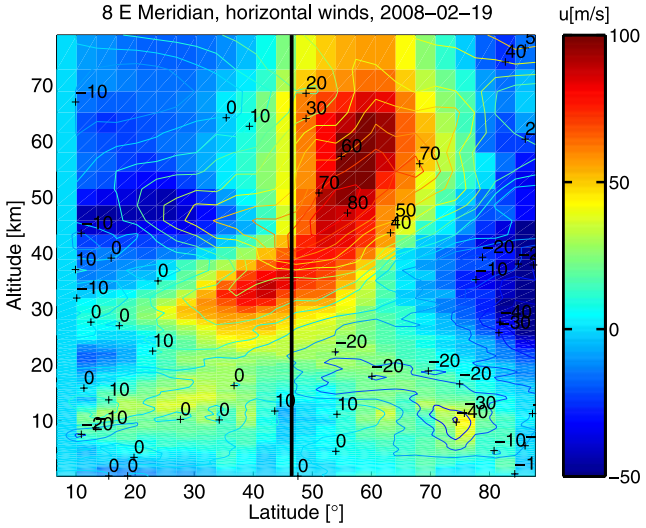

Figure 12. Cross section of ECMWF horizontal wind profiles along the 8°E meridian on 19 February. Contour lines represent meridional wind speed in m/s (positive values are northward). Color displays the zonal component with positive values being eastward. Two maxima of the so-called polar night jet are visible: one is at 30 km and 40°N and the second spreads from 50 to 65 km between 55° and 60°N. The polar night jet marks the edge of the polar vortex, which is normally located north of 60°N in winter. Hence one can see the displacement of the vortex toward the latitude of Bern, which is marked by the black line. Furthermore one observes the reversal of the zonal wind to westward between 20 and 60 km north of 65°N, which is characteristic for a major SSW.

and a HO_x cycle. The rate-determining reactions of these four cycles are the reactions of atomic oxygen O with NO_2, ClO, O_3, or HO_2, respectively. As a consequence, the ozone destruction rate and hence the ozone mixing ratio, is strongly dependent on the mixing ratio of atomic oxygen O. The O mixing ratio is determined by the O production (by O_3 photolysis, insensitive to temperature) and O destruction. Oxygen destruction occurs by the reaction

$$O + O_2 + M \longrightarrow O_3 + M. \quad (1)$$

[37] Such a three-body reaction is temperature dependent. A temperature increase as observed during the SSW results in a decrease of the reaction rate constant of reaction (1) by a factor of approximately 2. This leads to a significantly higher mixing ratio of atomic oxygen O and a smaller O_3 mixing ratio.

[38] The rate of the dominant NO_x cycle also depends on the NO_2 concentration and thus on the partitioning between NO and NO_2. The latter is mainly determined by the photolysis of NO_2 and the reaction

$$NO + O_3 \longrightarrow NO_2 + O_2. \quad (2)$$

[39] The rate constant of this ozone depleting reaction strongly increases with temperature. The effect on the ozone mixing ratio is smaller than that of reaction (1), but still significant.

[40] In order to illustrate the reasons of the above-described temperature sensitivity of ozone, we performed two additional model runs, shown in Figure 14. For this, the model run along the original trajectory was repeated, but with the temperature fixed at 248 K for the calculation of the rate coefficients of individual reactions: $O + O_2 + M \longrightarrow O_3 + M$ (green line) or $NO + O_3 \rightarrow NO_2 + O_2$ (blue line). If we compare those lines with the red lines (“No warming” and “Warming”), which are the same as in Figure 13, it turns out that more than half of the temperature sensitivity of ozone can be explained by reaction (1) and one third can be assigned to reaction (2).

[41] The above findings are consistent with early model results by *Stolarski and Douglass* [1985]. They showed that the temperature sensitivity of ozone in the altitude range of 30 km to 40 km is dominated by the temperature sensitivity of the NO_x catalytic ozone destruction cycle.

[42] Additional contributions to the observed variability of O_3 VMR can result from the transport of O_3 on a timescale shorter than the O_3 lifetime. Moreover, the mixing ratios of NO_y, Cl_y, and H_2O (and hence HO_x) may also be influenced by transport processes. This in turn leads to

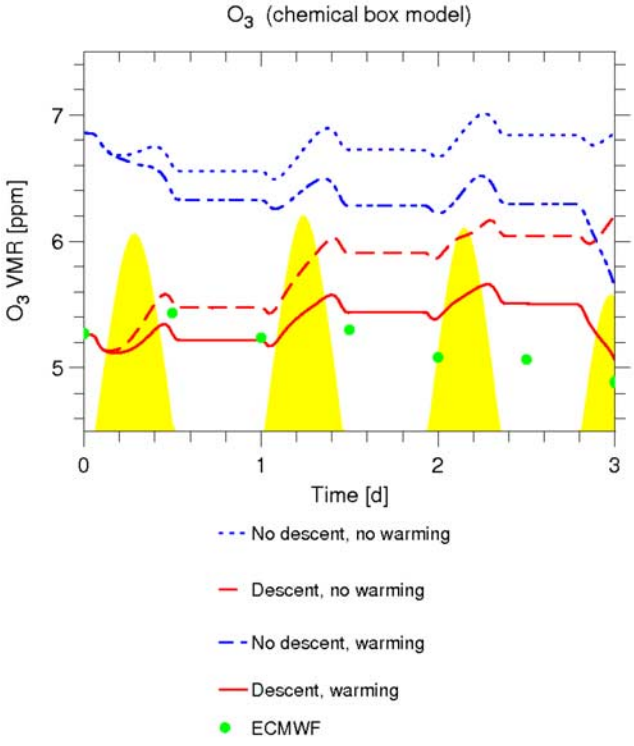

Figure 13. O_3 VMR, calculated by a chemical box model. Red curves (“Descent”) represent the O_3 VMR along the 1400 K trajectory of Figure 11. Blue curves (“No descent”) assume the same latitudes and longitudes, but a constant pressure level of 4 hPa. “Warming” refers to the original temperature along the trajectory. “No warming” assumes a constant temperature of 248 K. Green dots represent the ozone mixing ratio from ECMWF analyses along the trajectory. Warming accounts for about 2/3 of the observed ozone reduction.

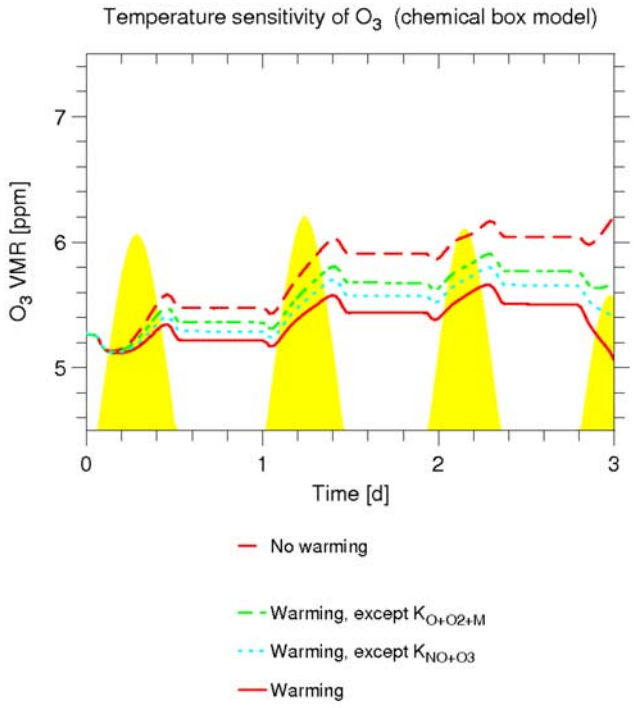

Figure 14. Temperature sensitivity of O_3 for the same situation as in Figure 13. The red curves show simulations with warming (taken into account for all reaction rate coefficients; full line) and without warming (T = 248 K = const.; dashed line). In order to demonstrate the role of individual reactions, the "warming" run was repeated, but with the temperature fixed at 248 K for the calculation of the rate coefficients of individual reactions: $O + O_2 + M \rightarrow O_3 + M$ (green line) or $NO + O_3 \rightarrow NO_2 + O_2$ (blue line). This shows that more than half of the temperature sensitivity of ozone is due to the first-mentioned reaction and about 1/3 is due to the latter one.

changes of the O_3 mixing ratio via the catalytic cycles mentioned above.

5. PSC Observed at Midlatitudes During SSW

[43] Strong ozone depletion during a SSW is surprising because the occurence of SSW is part of the reason why there is no strong ozone hole forming over the Arctic as there is one over the Antarctic. In fact, strong mixing of polar and low latitude air together with the temperature increase during a SSW prevents the development of very low temperatures and the build up of a strong and isolated polar vortex. Hence polar stratospheric clouds (PSCs) responsible for considerable ozone destruction are less abundant in the Arctic winter than in the Antarctic.

[44] PSC observations at midlatitudes are unusual. *Keckhut et al.* [2007] observed a PSC over southern France during a SSW in January 2006 by using a LIDAR. *Keil et al.* [2007] reported on very low ozone column densities over the UK for the same event. The ozone decrease was located in the upper troposphere and lower stratosphere. During the January 2006 SSW the polar vortex was shifted to North-West Europe and brought cold and ozone poor air. The same situation is observed in the current study of the major SSW 2008. *Rex et al.* [2006] reported on a trend toward colder extreme temperatures in the Arctic winter stratosphere. Colder temperatures lead to an increasing volume of air cold enough for the occurrence of PSCs, which in turn leads to more ozone loss inside the polar vortex. Arctic temperatures were observed in the stratosphere over Switzerland on 19 February 2008. The coldest temperature of 190 K was recorded on 19 February at 23 km altitude.

[45] Figure 15 shows the backscatter ratio measurements of CALIPSO along its orbit on 19 February 2008. It displays the altitude range of clouds with the location of the measurement (latitude, longitude) on the abscissa. The whitish area at an altitude of 20 to 25 km between 67°N and 49°N and 108°E and 2°W indicates the PSC. The parallel form of the high cloud at 10 km in the center of the image and the PSC suggests a connection of both by updrafts in the upper troposphere and lower stratosphere over England, also seen in Figure 11. The tropopause was lifted by an anticyclone, which led to the cooling below the threshold temperature for type 1a NAT PSC. This event is documented on a webpage of the UK Department for Environment as an ozone depletion event over England (http://www.ozone-uv.co.uk/ozone_events.php#Feb2008).

[46] PSCs play a major role in ozone depletion processes [*Crutzen and Arnold*, 1986]. Reactions occur on the surfaces of PSC particles that convert the reservoir forms of chlorine gases, $ClONO_2$ and HCl, to reactive forms, such as ClO, which lead to catalytic ozone destruction when sunlight is available. Large PSC particles may move downward because of gravity. Hence they remove HNO_3 from regions of the ozone layer. With less HNO_3, the highly reactive ClO remains chemically active for a longer period, thereby increasing chemical ozone destruction.

[47] Figure 16 shows a measurement of ClO and HNO_3 by the Aura/MLS satellite instrument for the 500 K isentrope during the SSW. Red color marks areas of high ClO VMR and magenta contours show regions of low HNO_3 VMR. The red solid line shows the orbit of the CALIPSO cloud and aerosol backscatter LIDAR. White vectors represent ECMWF horizontal wind speeds to illustrate the position of the polar vortex which reaches Southern Europe and North Africa. The largest wind vectors correspond to a speed of 60 m/s and mark the edge of the polar vortex. One observes a great area spread over Scandinavia, Great Britain, northern Germany and Poland with high values of ClO of up to 1.6 ppb. They come along with reduced nitric acid (HNO_3 VMR below 5 ppb are displayed by the narrow magenta contours). The coincidence of high ClO and low HNO_3 together with the low temperatures at 20 km illustrated in Figure 5 is conform with CALIPSO's observation of a PSC over England as indicated by the white part of the red orbit. Trajectory calculations show vertical updrafts in the lower stratosphere over England. Adiabatic cooling of the ascending humid air leads to the observed PSC.

[48] As a result the measured ozone decrease (Figure 8) in the lower stratosphere can be explained by the cold and ozone-poor polar vortex air shifted to Switzerland. Chemical reactions inside the polar vortex may have decreased the O_3 VMR already before the major SSW. Air rose by more than 2 km and cooled down from 212 K over the pole to 189 K over France, see Figure 11. The upwelling of

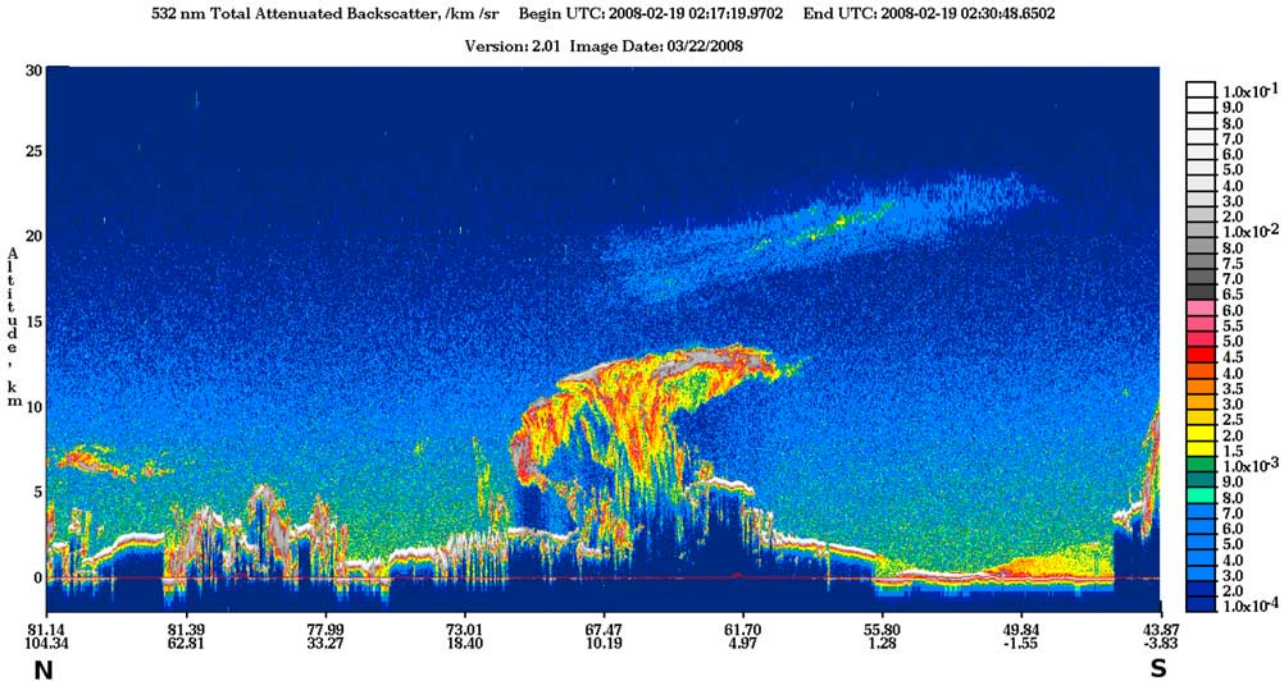

Figure 15. CALIPSO cloud image on an orbit across Europe on 19 February 2008. The *Y* axis shows height from 0 to 30 km and the *X* axis shows latitude and longitude from 81°N to 44°N and 104°E to 4°W, respectively. The picture shows the cloud coverage along the orbit which is drawn in Figure 16. A thin PSC cloud is visible (whitish area) at a 20-km altitude between 66°N and 49°N. The PSC base height increases southward. The parallel form of the high cloud at 10 km and the PSC suggests a connection of both due to the observed upwelling (Figure 11).

the tropopause and isentropes of the lower stratosphere (Figure 3) simultaneously occur with the shift of the polar vortex. The presence of a PSC over England however explains only a small fraction of the depletion by catalytic ozone destruction. Maximum losses of ozone at 500 K due to PSC were reported to be 60 ppb/d [*Rex et al.*, 2002] which alone cannot be responsible for the observed decrease of 0.6 ppm at Bern.

6. Conclusions

[49] Measurements from ground-based radiometers, radiosondes, and new satellite missions revealed a detailed picture of the spatiotemporal appearance of a major sudden stratospheric warming in February 2008. The most fascinating result was the clear coupling of all atmospheric layers by the major SSW, reaching from tropospheric upwelling (impressively seen in ECMWF and CALIPSO data in Figures 1 and 16) to mesospheric cooling (Figure 1). It is still an open and important question if SSWs and tropospheric blockings are interrelated. The major SSW of February 2008 clearly suggests to answer the question by "yes." A statistical study by *Martius et al.* [2009] found a strong correlation between upper tropospheric blockings and SSWs. High-quality measurements and data analysis can lead to the right ideas on the coupling mechanisms.

[50] In the lower stratosphere, a PSC was generated by updrafts over England and Scandinavia when the polar vortex was shifted during the SSW on 19 February 2008. The combined analysis of cloud data from CALIPSO and

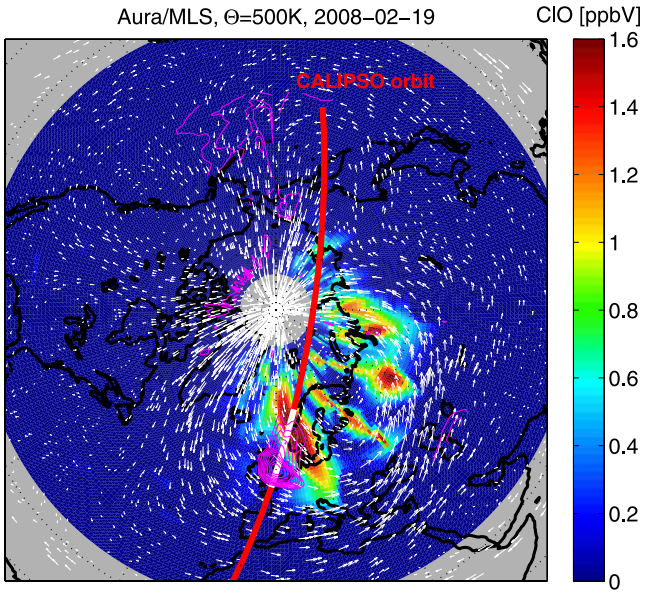

Figure 16. ClO (color) and HNO_3 (magenta contours show HNO_3 less than 5 ppbV) measured by Aura/MLS on 19 February at Θ = 500 K. There is a large area of enhanced ClO (red) and reduced HNO_3 over England and Scandinavia. The CALIPSO lidar detected a PSC over the white segment of the red orbit line in the European sector. The white arrows denote horizontal wind vectors from ECMWF. The strongest winds (longest arrows) indicate the position of the vortex edge. Regions of high ClO are observed within the polar vortex.

chemistry data from Aura/MLS permitted the clear identification and localization of the PSC. The PSC occurred, rather unusual, at midlatitudes. This confirms the possibility of the existence of PSCs at midlatitudes during SSW as already observed over France during the 2006 SSW [*Keckhut et al.*, 2007].

[51] Now we summarize the results from observations, trajectory calculations, and simulations in order to give a comprehensive and detailed picture: The Northern Hemisphere winter stratosphere was strongly disturbed in January and Februray 2008 with two minor SSW (16 and 31 January) and one major SSW (17 February). During the major SSW, temperatures above Bern increased by up to 70 K at altitudes between 35 and 50 km (maximum increase was at 4 hPa). At the same time, a pronounced cooling was observed in the lower stratosphere between 20 and 25 km. Temperatures fell below the PSC type 1a threshold of 195 K, and a PSC was observed by CALIPSO over Scandinavia and England (southermost latitude of the PSC was 49°N). The ground-based microwave radiometer GROMOS observed a reduction of the O_3 VMR between 20 and 50 km altitude over Bern.

[52] The reasons of the observed ozone depletion were investigated by means of trajectory calculations and numerical modeling. In the lower stratosphere cold ozone-poor polar vortex air was transported to Switzerland (Figure 11). Additionally lower stratospheric ozone was depleted to some extent by the observed PSC over England (Figure 15). Trajectory analyses proved that the PSC was caused by adiabatic cooling due to updrafts in the upper troposphere and lower stratosphere on 19 February.

[53] A strong vertical temperature gradient occurred at about 10 hPa. Above 10 hPa, the SSW was accompanied by a sudden temperature increase of up to 70 K. This temperature increase is solely due to adiabatic heating of descending air masses (Figure 11). The chemical box model showed that the temperature increase causes a faster ozone destruction due to the temperature dependences of the reaction rate coefficients. The chemical ozone destruction is dominated by the catalytic NO_x cycle, which is more efficient at higher temperatures. Simulations led to the conclusion that about 2/3 of the observed O_3 decrease at 4 hPa can be explained by the temperature increase.

[54] A strong wind shear occurred at 5 hPa suggesting a meridional circulation cell during the SSW (Figure 12). The two different wind systems led to air mass exchange of polar and subtropical air. Polar air is transported upward to midlatitudes below 5 hPa. Above 5 hPa air parcels move downward from low to high latitudes. Adiabatic cooling and warming are the consequences and led to the large vertical gradient in stratospheric temperature above Bern.

[55] The major SSW was associated with water vapor enhancements in the upper troposphere (Aura/MLS, CALIPSO), stratosphere, and mesosphere (MIAWARA, Aura/MLS) over Europe. The enhancements could be explained by transport to Switzerland of H_2O out of regions with higher VMR. The formation of the PSC over England and Scandinavia was enabled by the humid air of the polar vortex. The present study marginally discussed the role of water vapor during the SSW. The CALIPSO cloud image suggests that water vapor convection and transport processes of upper tropospheric water vapor by planetary wave breaking could be a key to understand and predict a SSW [*Coy et al.*, 2009].

[56] A recent study by *Charlton-Perez et al.* [2008] shows an increase of the frequency of major stratospheric warmings in the 21st century. Sudden stratospheric warmings influence the whole atmosphere and are essential for estimation of future ozone and temperature trends. *Newman* [2009] reveals the possibility of a stratospheric influence on midlatitude winter weather: During the SSW at the end of January 2009 the vortex split up in two cells, one was shifted to North America and one to the east of Europe. Both induced changes in tropospheric wind patterns and led to heavy and unusual snow falls over western Europe from France to England and also in the south of the United States. Simultaneously our radiometer detected again a decrease of O_3 and enhancement of H_2O in the stratosphere during the SSW. A mesospheric water vapor increase even preceded the SSW 2009 by a few days. Hence further monitoring of middle atmospheric trace gases as H_2O and O_3 will continue and is mandatory for quantitative investigations of the role of SSWs for atmospheric circulation and chemistry.

[57] **Acknowledgments.** This work has been funded by the Swiss National Science Foundation under grant 200020-115882, MeteoSwiss in the frame of the Swiss GAW-project SHOMING, and the Oeschger Centre for Climate Research. We are grateful for the data access to ECMWF operational analysis and NASA's satellite experiments Aura/MLS, CALIPSO, and TIMED/SABER. A special thank to Gabriele Stiller from Forschungszentrum Karlsruhe who provided MIPAS NO_2 profiles for the chemical box model. We thank the anonymous reviewers, their constructive comments led to an improvement of the article.

References

Brasseur, G. P., J. J. Orlando, and G. S. Tyndall (1999), *Atmospheric Chemistry and Global Change*, Oxford Univ. Press, New York.

Calisesi, Y., H. Wernli, and N. Kämpfer (2001), Midstratospheric ozone variability over Bern related to planetary wave activity during the winters 1994–1995 to 1998–1999, *J. Geophys. Res.*, *106*, 7903–7916.

Chaffey, J., and J. Fyfe (2001), Arctic polar vortex variability in the Canadian middle atmosphere model, *Atmos.-Ocean*, *39*, 457–469.

Charlton, A. J., and L. M. Polvani (2007), A new look at stratospheric sudden warmings: Part I. Climatology and modeling benchmarks, *J. Clim.*, *20*(3), 449–469, doi:10.1175/JCLI3996.1.

Charlton-Perez, A. J., L. M. Polvani, J. Austin, and F. Li (2008), The frequency and dynamics of stratospheric sudden warmings in the 21st century, *J. Geophys. Res.*, *113*, D16116, doi:10.1029/2007JD009571.

Charyulu, D. V., V. Sivakumar, H. Bencherif, G. Kirgis, A. Hauchecorne, P. Keckhut, and D. Narayana Rao (2007), 20-year lidar observations of stratospheric sudden warming over a midlatitude site, observatoire de haute provence (OHP and 44°N, 68°E): Case study and statistical characteristics, *Atmos. Chem. Phys. Discuss.*, *7*(6), 15,739–15,779.

Chau, J. L., B. G. Fejer, and L. P. Goncharenko (2009), Quiet variability of equatorial E × B drifts during a sudden stratospheric warming event, *Geophys. Res. Lett.*, *36*, L05101, doi:10.1029/2008GL036785.

Coy, L., S. Eckermann, and K. Hoppel (2009), Planetary wave breaking and tropospheric forcing as seen in the stratospheric sudden warming of 2006, *J. Atmos. Sci.*, *66*, 495–507.

Crutzen, P. J., and F. Arnold (1986), Nitric acid cloud formation in the cold antarctic stratosphere — a major cause for the springtime "ozone hole", *Nature*, *324*, 651–655, doi:10.1038/324651a0.

Deuber, B., A. Haefele, D. G. Feist, L. Martin, N. Kämpfer, G. E. Nedoluha, V. Yushkov, S. Khaykin, R. Kivi, and H. Vömel (2005), Middle Atmospheric Water Vapour Radiometer (MIAWARA: Validation and first results of the LAUTLOS/WAVVAP campaign, *J. Geophys. Res.*, *110*(D13), D13306, doi:10.1029/2004JD005543.

Draxler, R., and G. Hess (1998), An overview of the Hysplit 4 modeling system for trajectories, dispersion and deposition, *Aust. Met. Mag.*, *47*, 295–308.

Flury, T. (2008), TomToM:Toms Trajectory Model, Version 1, *IAP Res. Rep. 2008-07-MW*, Institut für angewandte Physik, Univ. Bern, Bern, Switzerland.

Flury, T., S. C. Müller, K. Hocke, and N. Kämpfer (2008), Water vapor transport in the lower mesosphere of the subtropics: A trajectory analysis, *Atmos. Chem. Phys.*, *8*(23), 7273–7280.

Froidevaux, L., et al. (2008), Validation of aura microwave limb sounder stratospheric ozone measurements, *J. Geophys. Res.*, *113*, D15S20, doi:10.1029/2007JD008771.

Haefele, A., E. D. Wachter, K. Hocke, N. Kämpfer, G. E. Nedoluha, R. M. Gomez, P. Eriksson, P. Forkman, A. Lambert, and M. J. Schwartz (2009), Validation of ground based microwave radiometers at 22 GHz for stratospheric and mesospheric water vapor, *J. Geophys. Res.*, doi:10.1029/2009JD011997, in press.

Hanson, D., and K. Mauersberger (1988), Laboratory studies of the nitric acid trihydrate: Implications for the south polar stratosphere, *Geophys. Res. Lett.*, *15*, 855–858.

Hirooka, T., T. Ichimaru, and H. Mukougawa (2007), Predictability of stratospheric sudden warmings as inferred from ensemble forecast data: Intercomparison of 2001/02 and 2003/04 winters, *J. Meteorol. Soc. Jpn.*, *85*(6), 919–925.

Hoffmann, P., W. Singer, D. Keuer, W. K. Hocking, M. Kunze, and Y. Murayama (2007), Latitudinal and longitudinal variability of mesospheric winds and temperatures during stratospheric warming events, *J. Atmos. Sol.-Terr. Phys.*, *69*, 2355–2366, doi:10.1016/j.jastp.2007.06.010.

Hoppel, K. W., N. L. Baker, L. Coy, S. D. Eckermann, J. P. McCormack, G. E. Nedoluha, and D. E. Siskind (2008), Assimilation of stratospheric and mesospheric temperatures from MLS and SABER into a global NWP model, *Atmos. Chem. Phys.*, *8*(20), 6103–6116.

Keckhut, P., C. David, M. Marchand, S. Bekki, J. Jumelet, A. Hauchecorne, and M. Höpfner (2007), Observation of polar stratospheric clouds down to the Mediterranean coast, *Atmos. Chem. Phys.*, *7*(19), 5275–5281.

Keil, M., D. R. Jackson, and M. C. Hort (2007), The January 2006 low ozone event over the UK, *Atmos. Chem. Phys.*, *7*, 961–972.

Kleinböhl, A., J. Kuttippurath, M. Sinnhuber, B.-M. Sinnhuber, H. Küllmann, K. Künzi, and J. Notholt (2005), Rapid meridional transport of tropical airmasses to the Arctic during the major stratospheric warming in January 2003, *Atmos. Chem. Phys.*, *5*(23), 1291–1299.

Labitzke, K. (1981), Stratospheric-mesospheric midwinter disturbances: A summary of observed characteristics, *J. Geophys. Res.*, *86*, 9665–9678.

Lait, L. R. (1994), An alternative form for potential vorticity, *J. Atmos. Sci.*, *51*, 1754–1759, doi:10.1175/1520-0469(1994)051.

Lambert, A., et al. (2007), Validation of the aura microwave limb sounder middle atmosphere water vapor and nitrous oxide measurements, *J. Geophys. Res.*, *112*, D24S36, doi:10.1029/2007JD008724.

Limpasuvan, V., D. W. J. Thompson, and D. L. Hartmann (2004), The life cycle of the Northern hemisphere sudden stratospheric warmings, *J. Clim.*, *17*, 2584–2597.

Liu, H.-L., and R. G. Roble (2002), A study of a self-generated stratospheric sudden warming and its mesospheric-lower thermospheric impacts using the coupled TIME-GCM/CCM3, *J. Geophys. Res.*, *107*(D23), 4695, doi:10.1029/2001JD001533.

Liu, Y., C. X. Liu, H. P. Wang, X. Tie, S. T. Gao, D. Kinnison, and G. Brasseur (2009), Atmospheric tracers during the 2003 2004 stratospheric warming event and impact of ozone intrusions in the troposphere, *Atmos. Chem. Phys.*, *9*, 2157–2170.

Manney, G. L., et al. (2009), Satellite observations and modelling of transport in the upper troposphere through the lower mesosphere during the 2006 major stratospheric sudden warming, *Atmos. Chem. Phys. Discuss.*, *9*(2), 9693–9745.

Martius, O., L. M. Polvani, and H. C. Davies (2009), Blocking precursors to stratospheric sudden warming events, *Geophys. Res. Lett.*, *36*, L14806, doi:10.1029/2009GL038776.

Matsuno, T. (1971), A dynamical model of the stratospheric sudden warming, *J. Atmos. Sci.*, *28*, 1479–1494, doi:10.1175/1520-0469(1971)028.

McGill, M. J., M. A. Vaughan, C. R. Trepte, W. D. Hart, D. L. Hlavka, D. M. Winker, and R. Kuehn (2007), Airborne validation of spatial properties measured by the CALIPSO lidar, *J. Geophys. Res.*, *112*, D20201, doi:10.1029/2007JD008768.

McInturff, R. (1978), Stratospheric warmings: Synoptic, dynamic and general-circulation aspects, *NASA Reference Publ. NASA-RP-1017*, NASA, Natl. Meteorol. Cent., Washington, D. C.

Newman, P. (2009), Stratosphere Influences Winter Weather, *NASA Earth Observatory*, NASA, http://earthobservatory.nasa.gov/IOTD/view.php?id=36972.

Remsberg, E., et al. (2003), On the verification of the quality of SABER temperature, geopotential height, and wind fields by comparison with met office assimilated analyses, *J. Geophys. Res.*, *108*(D20), 4628, doi:10.1029/2003JD003720.

Rex, M., et al. (2002), Chemical depletion of arctic ozone in winter 1999/2000, *J. Geophys. Res.*, *107*(D20), 8276, doi:10.1029/2001JD000533.

Rex, M., et al. (2006), Arctic winter 2005: Implications for stratospheric ozone loss and climate change, *Geophys. Res. Lett.*, *33*, L23808, doi:10.1029/2006GL026731.

Sander, S. P., et al. (2006), *Chemical Kinetics and Photochemical Data for Use in Atmospheric Studies*, *Evaluation No. 15 (JPL Publication 06-2)*, Jet Propulsion Laboratory, Pasadena, Calif.

Scherhag, R. (1952), Die explosionsartige Stratosphärenerwarmung des Spätwinters 1951/52, *Ber. Deutsch. Wetterdienstes*, *38*, 51–63.

Schoeberl, M. R. (1978), Stratospheric warmings: Observations and theory, *Rev. Geophys.*, *16*, 521–538.

Schoeberl, M., and L. Sparling (1994), Trajectory modelling, *Diagnostic Tools in Atmospheric Physics, Proc. S.I.F. Course CXVI.*

Siskind, D. E., L. Coy, and P. Espy (2005), Observations of stratospheric warmings and mesospheric coolings by the TIMED SABER instrument, *Geophys. Res. Lett.*, *32*, L09804, doi:10.1029/2005GL022399.

Sonnemann, G. R., M. Grygalashvyly, and U. Berger (2006), Impact of a stratospheric warming event in January 2001 on the minor constituents in the MLT region calculated on the basis of a new 3D-model LIMA of the dynamics and chemistry of the middle atmosphere, *J. Atmos. Sol.-Terr. Phys.*, *68*, 2012–2025, doi:10.1016/j.jastp.2006.04.005.

Stolarski, R. S., and A. R. Douglass (1985), Parameterization of the photochemistry of stratospheric ozone including catalytic loss processes, *J. Geophys. Res.*, *90*, 10,709–10,718.

Sun, L., and W. A. Robinson (2009), Downward influence of stratospheric final warming events in an idealized model, *Geophys. Res. Lett.*, *36*, L03819, doi:10.1029/2008GL036624.

Waters, J. W., et al. (2006), The earth observing system microwave limb sounder (EOS MLS) on the aura satellite, *IEEE Trans. Geosci. Remote Sens.*, *44*, 1075–1092, doi:10.1109/TGRS.2006.873771.

Wetzel, G., et al. (2007), Validation of MIPAS-ENVISAT NO2 operational data, *Atmos. Chem. Phys.*, *7*, 3261–3284.

Winker, D. M., W. H. Hunt, and M. J. McGill (2007), Initial performance assessment of CALIOP, *Geophys. Res. Lett.*, *34*, L19803, doi:10.1029/2007GL030135.

T. Flury, A. Haefele, K. Hocke, and N. Kämpfer, Institute of Applied Physics, University of Bern, Sidlerstrasse 5, CH-3012 Bern, Switzerland. (thomas.flury@iap.unibe.ch)

R. Lehmann, Alfred Wegener Institute for Polar and Marine Research, Telegrafenberg A43, D-14473 Potsdam, Germany.